Application of Laser Doppler Velocimetry to unsteady flow around rotating blades

E. Berton, M. Nsi Mba, D. Favier, C. Maresca

L.A.B.M. Laboratory (ex IRPHE/ASI Laboratory), UMSR 2164 of CNRS, University of Méditerranée
163 Avenue de Luminy, case 918, 13009 Marseille, France

ABSTRACT

New computational tools associated with new numerical and experimental methods have mainly improved the understanding of rotary wing aerodynamics resulting in better performances. Nevertheless some challenging problems remain to be solved with more accuracy. So are the precise prediction of the wake structure, the formation and shedding of tip vortices from blades, and the features of the flow close and around the blade. Concerning new experimental methods, the non-intrusive nature of the Laser Doppler Velocimetry has allowed many experimental works around and in the wake of rotating blades. Recently, velocity profiles measured around and in the boundary layer of a blade began to appear in the literature. As the techniques seems to be got under control in the case of axisymmetric flow, some effort remains to be paid in the case of phase dependent rotating flow. Particularly, the knowledge of the velocity field around the blade of a helicopter rotor in forward flight is of prime interest for qualitative and quantitative purposes. The experimental method presented here has tackled this challenge.

In fact, the present paper concerns a new approach of forces (lift and drag) measurement, acting on the profile of a rotor helicopter blade in forward flight. The method is based on the use of the momentum equation in which all terms are expressed by means of the velocity field measured by a Laser Doppler Velocimeter (LDV) technique. The 3D velocity field has been determined upstream, downstream and around a blade profile by means of a long focal length LDV. The experiments, conducted in a large close section wind tunnel (see Figure 1) on a helicopter rotor model in forward flight ($\mu = 0.20$), have been realized for a radial position $r/R = 0.70$ of the blade located in the advancing and retreating zones (respectively at $\Psi_b = 90$ deg and 270 deg). On a basic point of view, the section of the blade is considered as a fixed ptofile in a fictitious 2D flow where the momentum equation is applied with success to evaluate the lift and drag forces.

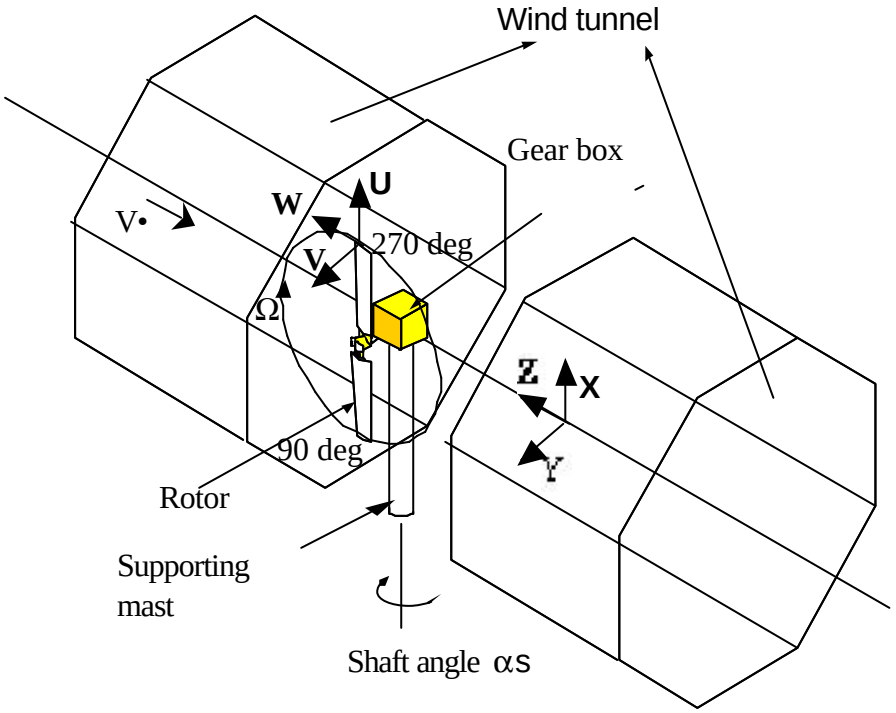

Fig. 1. Scheme of the experimental set-up in the wind-tunnel

1. NOMENCLATURE

b	Number of blades
c	Constant blade chord, (m)
C_L	Profile blade lift coefficient
C_D	Profile blade drag coefficient
$\vec{q}$	Velocity vector (components U,V,W, defined in Fig.1)
r	Radial distance from the rotation axis, (m)
R	Rotor blade radius, (m)
Re	Reynolds number, ($Re=V_\infty c/\nu$)
$\vec{V}$	Velocity vector in the grid plane, (m/s)
Vi	Induced velocity through the rotor disc, (m/s)
V_T	Rotational tip speed ($V_T = ?R$), m/s
α_S	Shaft angle, (deg)
β	Flapping angle, (deg)
Γ	Blade circulation along the span, (m^2/s)
θ	Collective pitch angle at r/R=0.75, (deg)
θi	Induced angle of incidence, (deg)
Ω	Angular rotational frequency, (rad/s)
Ψ_b	Angular blade position, (deg)
ρ, ρ_∞	Density, (kg/m^3)

2. INTRODUCTION

The accurate prediction of spanwise airloads distribution and flowfield on helicopter rotor blades remains of primary importance for improving rotor aerodynamics performances (Landgrebe, 1986, Johnson, 1986, McCroskey, 1988 and Chen and McCroskey, 1988), particularly the drag coefficient, conditioning the power to request from the engines in the different capabilities of flights (hover, forward, climb or descent). During the last decades, the development of numerical analysis and experimental methodologies have substantially improved the blade distribution circulation and the drag profile prediction, especially in hovering configurations (Maresca et al., 1986, Silva et al., 1993, Ramos et al., 1994). However, an equivalent contribution remains to be provided in the case of advancing configurations. Some recent experiments, performed in hover (Berton et al., 1994 and McAlister et al., 1995), have shown that the momentum equation and the Kutta-Joukovsky theorem have made possible the calculation of the blade profile lift and drag including viscous effects, by only use of the velocity field around and in the wake of the profile. The method, taking advantage of the axisymmetry of the flow in hover, can ignore the pressure distribution field and unsteady terms so that the equations of C_L and C_D only involve velocities distribution. In the case of an advancing rotor configuration, the axisymmetry of the flow disappears giving rise to pressure terms in the momentum equation. Nevertheless, it remains possible, so long as the incompressible case is considered, to connect the unsteady and pressure terms to local velocities via the Bernoulli's equation, introducing however the $\partial\varphi/\partial t$ term. This term, and more precisely the term $\partial(\varphi_\infty-\varphi_M)/\partial t$, can be replaced by the integral of the quantity $\vec{V}.\vec{dl}$ along a streamline between M and ∞ (M is a point of the control surface where the momentum equation is applied).

The first part of the present paper deals with the determination of force components deduced from the momentum equations applied to a contour suitable for forward flight. It is shown that the different terms concerned can be expressed in terms of local velocities by help of finite differences and Bernoulli equation. In the second part of the paper, experimental set up and velocity measurement technique are described. They have allowed the acquisition of a data base corresponding to velocities measured in a contour surrounding the blade at a given r/R. In the third part of the paper are compared the different terms involved by the components of the aerodynamic force acting on the blade at r/R=0.7 and Ψ_b= 90 deg and 270 deg, in the case of an advancing parameter μ=0.20. The drag and lift coefficients are so deduced from the momentum equation, and the lift is also determined by use of the Kutta-Joukovsky law. These results are compared to those obtained in the simplified case where volume terms and spanwise effects are neglected. Are also compared results deduced from 2D steady polar.

3. AERODYNAMIC FORCES DEDUCED FROM THE MOMENTUM EQUATIONS

When using the unsteady incompressible momentum equations applied to a contour as defined in Figure 2, the aerodynamic forces acting on the blade profile can be given by the equation :

$$\vec{F} = -\iiint_{v} \underbrace{\left[\frac{\partial r\vec{q}}{\partial t}\right]}_{(I)} + \underbrace{\vec{\Omega} \wedge r\vec{q}}_{(II)} \Big] dv - \underbrace{\iint_{S_\infty} r\vec{q}.(\vec{q}.d\vec{S})}_{(III)} - \underbrace{\iint_{S_\infty} p.\vec{n}d\vec{S}}_{(IV)} + \underbrace{\iiint_{v} r\vec{g}\, dv}_{(V)} \quad (1)$$

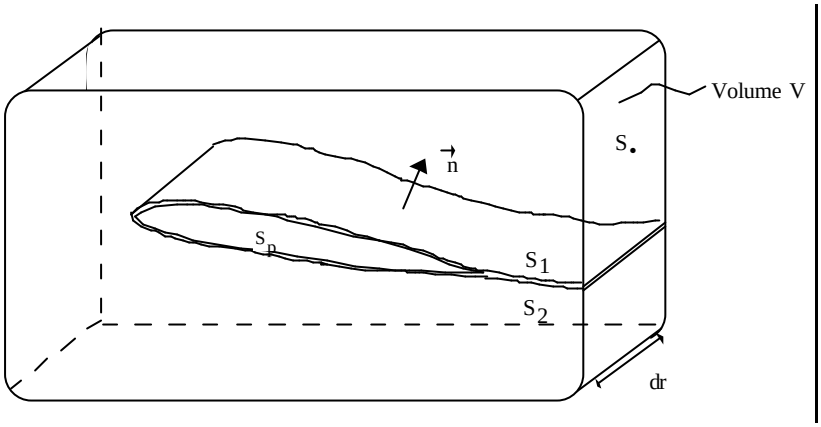

S_p = Blade section

S_1, S_2 = wake surface

S_8 = external surface

Fig. 2. Control volume surrounding the blade

3.1. Evaluation of term (I) : $\iiint_V \left[\frac{\partial r\vec{q}}{\partial t}\right] dV$

The derivative of the velocity vector can be written through the following finite difference:

$\frac{\partial \vec{q}(t)}{\partial t} = \lim_{t\to 0} \frac{\vec{q}(t+\Delta t) - \vec{q}(t-\Delta t)}{2\Delta t}$ providing the approximated value of term (I) :

$$\iiint_V \left[\frac{\partial r\vec{q}}{\partial t}\right] dv \approx r\sum_i \frac{\vec{q}_i(t+\Delta t) - \vec{q}_i(t-\Delta t)}{2\Delta t} dv \quad (2)$$

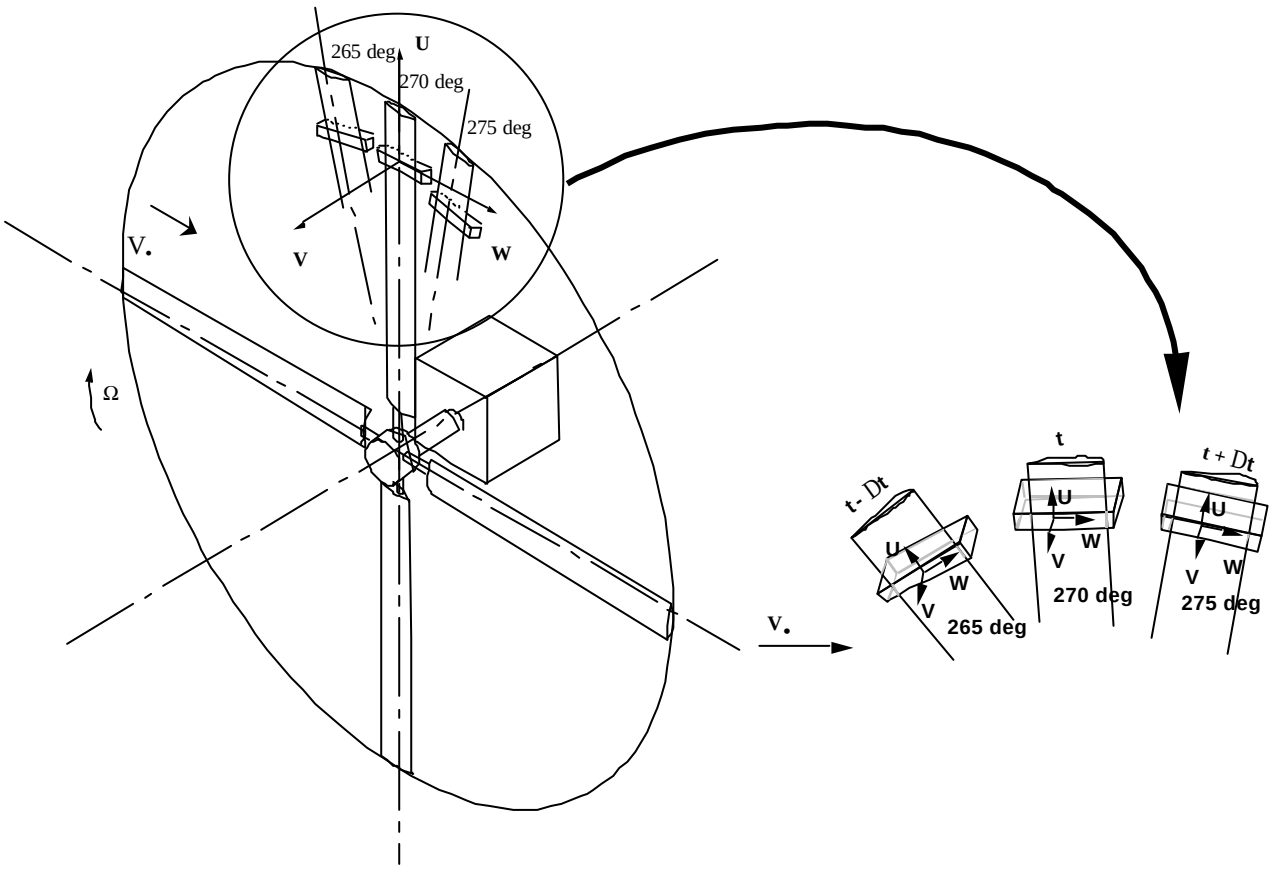

Fig. 3. Control volume at t, t+Dt, t-Dt, around the blade phase Y_b=270deg

The discretisation time Δt is determined with respect to the accuracy of the velocity measurement. It is shown that the variation of velocities can be measured with a good accuracy when : $\Delta\Psi_b=2\pi.\Delta t/T\approx 5$ deg (see Figure 3). The external section bounding the volume V is discretised on its lateral part by the following grid in Figure 4 :

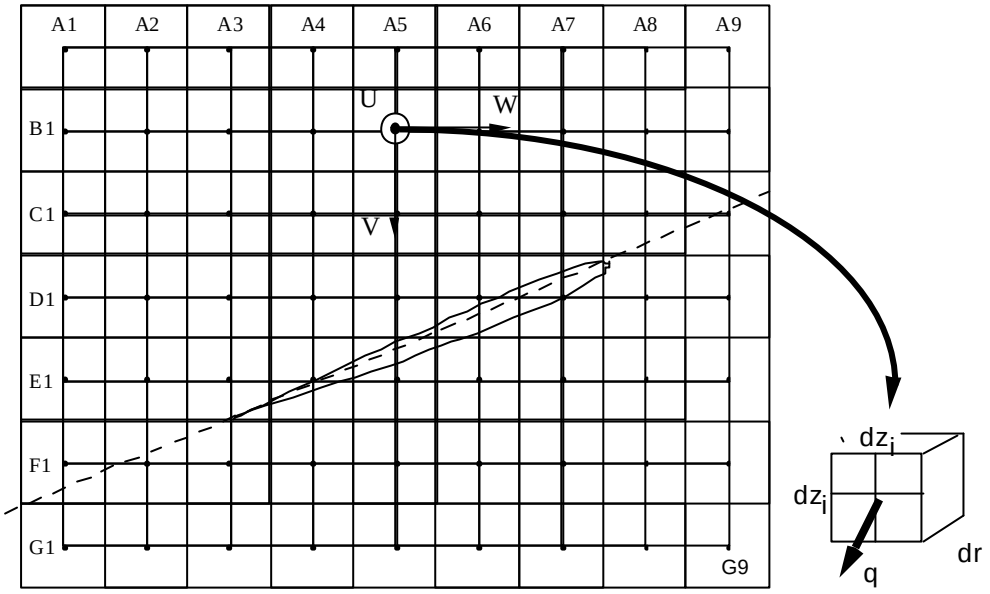

Fig. 4. Grid defining the lateral surface of V

The evaluation of the second term of equation (1) involves n elementary volumes, according to the grid defined above. The quantity $\vec{q}$ is considered for each elementary volume dv_i as the average between the velocities measured in the center of the square (dz_ixdz_i), at r and r+ Δr.

3.2. Evaluation of the inertial term (II) : $\iiint_V (\vec{\Omega} \wedge r\vec{q})dv_i$

In a fixed frame linked to the wind tunnel (see Figure 1), the rotational $\vec{\Omega}$ and the velocity vector $\vec{q}$ are given by :

$$\vec{\Omega} = \begin{bmatrix} 0 \\ \Omega\cos a_s \\ \Omega\sin a_s \end{bmatrix} \qquad \vec{q} = \begin{bmatrix} U \\ V \\ W \end{bmatrix}$$

The rotational velocity Ω is constant, and α_s is the shaft angle. The evaluation of term (II) is obtained at time t by integrating the experimental values of $\vec{\Omega} \wedge \vec{q}$ in the volume V .

3.3. Evaluation of term (III): $\iint_{S_\infty} r\vec{q}.(\vec{q}.d\vec{S})$

The knowledge of experimental velocities in the mesh of the grid previously shown allows to numerically calculate the value of term (III).

3.4. Evaluation of term (IV): $\iint_{S_\infty} p.\vec{n}dS$

In order to avoid the measurement of the pressure field on the bounding surfaces, it is proposed to approximate the time dependent Bernoulli equation by terms depending only on velocities. Particular attention is paid to the time-dependent term $\partial j / \partial t$.

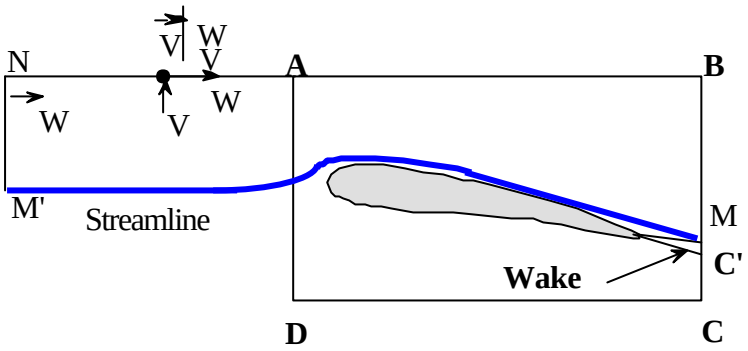

Fig. 5. Control volume for the pressure term determination

As shown in Figure 5, if M' is supposed to be at the infinity, the Bernoulli equation, applied along the streamline MM', gives : $p_M - p_\infty = \frac{1}{2} r (q_\infty^2 - q_M^2) + r \frac{\partial (j_\infty - j_M)}{\partial t}$

The integral (IV) concerning a closed surface can be written as follows :

$$\iint_{S_\infty} p.\vec{n}d\vec{S} = \iint_{S_\infty} (p - p_\infty).\vec{n}d\vec{S} = \iint_{S_\infty} \left[\frac{1}{2} r (q_\infty^2 - q^2) + r \frac{\partial (j_\infty - j)}{\partial t} \right] \vec{n}d\vec{S} \qquad (3)$$

Along the streamline MM', if we note $\vec{V} = -\overrightarrow{grad}\varphi$ the velocity vector in the grid plane, then : $j_M - j_\infty = \int_M^{M'} \vec{V}.d\vec{l} = \int_M^B V dy + \int_B^N W dz$, and the term $\partial(\varphi_\infty - \varphi_M)/\partial t$ can then be approximated by the finite difference equation :

$$\frac{\partial (j_\infty - j_M)}{\partial t} \approx \frac{\left(\sum_{MB} V_j dl \right)_{t+\Delta t} - \left(\sum_{MB} V_j dl \right)_t}{\Delta t} + \frac{\left(\sum_{BN} W_i dl \right)_{t+\Delta t} - \left(\sum_{BN} W_i dl \right)_t}{\Delta t} \qquad (4)$$

showing that the term (IV) can be expressed by only help of velocity measurements in the control contour.

The gravity term (V) of equation (1) is neglected as air flows are concerned.

4. EXPERIMENTAL FACILITIES AND MEASUREMENTS PROCEDURES

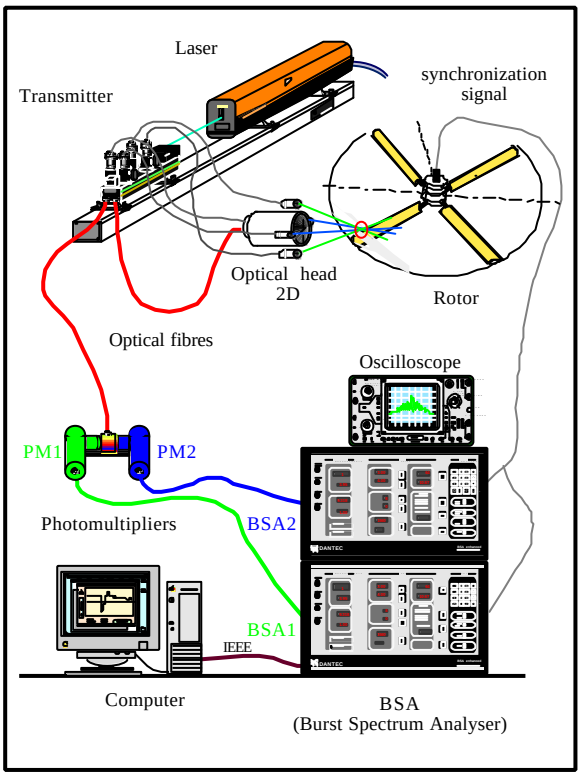

Fig. 6. Laser Velocimetry method used in the wind-tunnel

The model-scale of a two bladed rotor is set up on the test rig installed in the S1-Luminy wind-tunnel test section, 3m in diameter, and 100ms^{-1} in maximum velocity (see Figure 1). The test stand itself is mounted on an anti-vibration pad within the wind tunnel test hall. The rotor hub is mounted vertically by means of a supporting mast. The model-rotor consists of a fully articuled rotor hub which can be equipped with interchangeable sets of blades. For the purpose of the present study, the rotor system tested was a 2 bladed, 1.5 m diameter, with rectangular tip, OA209 profile blades, 0.05m in chord, rotating at a tip velocity V_T=107 ms^{-1}, in a wind speed of 21.4 ms^{-1}; the advancing parameter is μ=0.20. Several measurements techniques suited for surveying the flow in the near and far wake regions and around the blades have been developed (see Ramos et al., 1994, Berton et al., 1994) including a long focal (2m to 2,5m) Laser Velocimetry (LV) technique.

The three-dimensional velocity field around the blade is measured by a fiber optic laser velocimeter system performing two consecutive 2D measurements. In the vicinity of the blade the velocity components U,V and the axial component W are determined by LV in a fixed coordinates system. A glycerin-based smoke generator was used to seed the flow.

Use of a 500 steps encoder provides an azimuthal resolution of 0.72 deg. The velocities components are statistical averaged up to 200 samples per azimuthal step ($\Delta\Psi$=0.72 deg). Detailed characterization of the flowfield is made possible by a combination of the 0.1 mm step resolution afforded by the laser optics traverse and the 0.3 mm diameter of the LV system measuring volume. The initiation and synchronization of the instantaneous acquisition data are realized by means of a photo-cell delivering the azimuthal origin (Ψ = 0 deg).

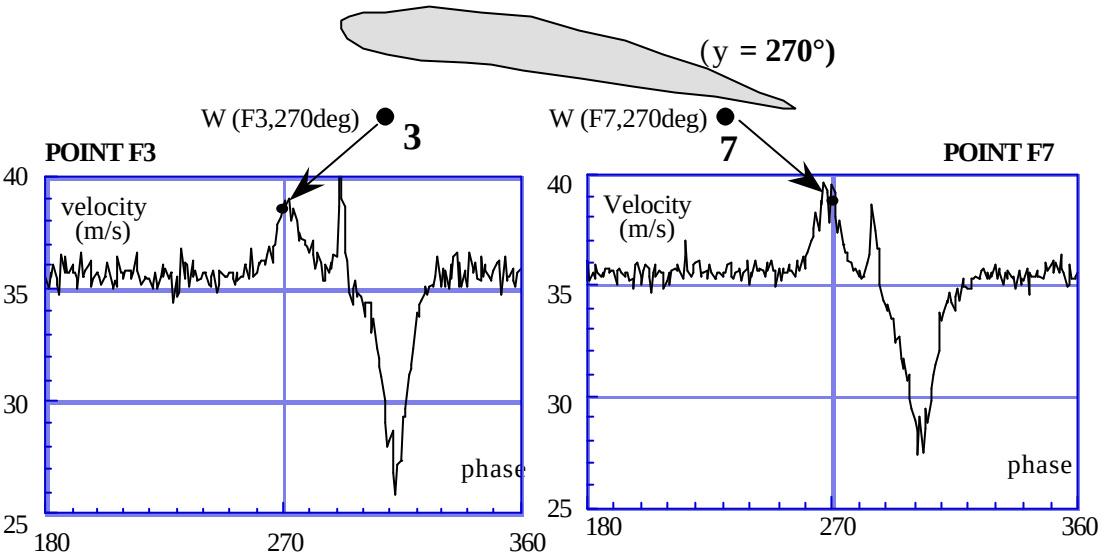

Fig. 7. Example of velocity records

Fig. 7 shows as an example the variations with Ψ of the W component at points F3 and F7 of the grid previously defined in Figure 4. The instantaneous values of W at these points for Ψ_b=270 are given by the corresponding values of the graph at the phase 270deg. The velocity components are so registered at 63 points of the grid with an accuracy of about 2% (see Berton et al., 1994), for 3 azimuthal positions of the blade (Ψ_b=270 deg, Ψ_b-$\Delta\Psi$=265 deg, and Ψ_b+$\Delta\Psi$=275 deg) and 2 radial positions (r=0.70R, and r+Δr=0.713R).

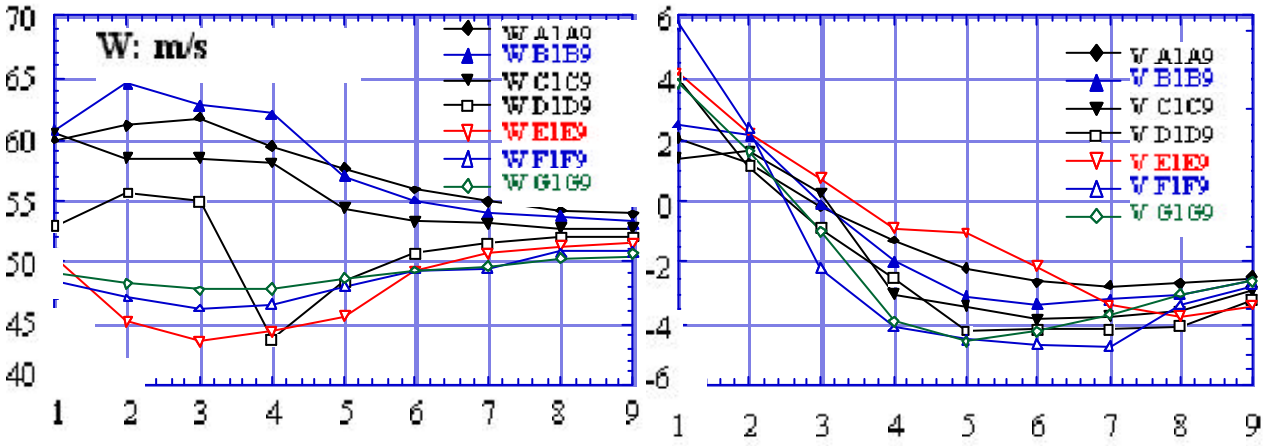

Fig. 8. V and W component variations along the grid lines at Y=270 deg

Fig. 8 and Fig. 9 show as an example, typical distributions of V and W obtained at Ψ=270 deg along lines and columns of the grid. The velocities are presented in a frame linked to the blade. It can be observed that the maxima of W occur on the upperside as expected, and the maxima velocity of the induced vertical velocity on the lower side.

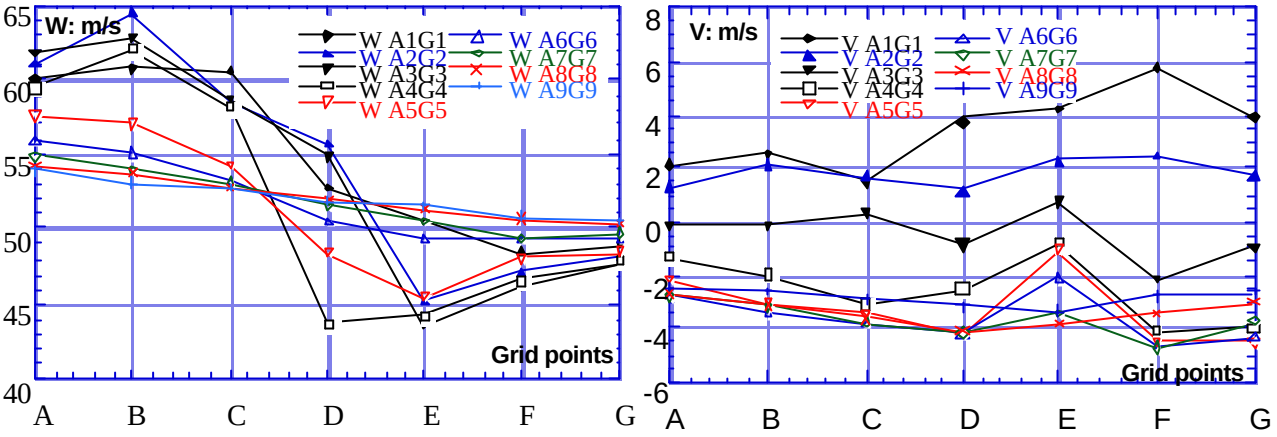

Fig. 9. V and W component variations along the grid columns at Y=270 deg

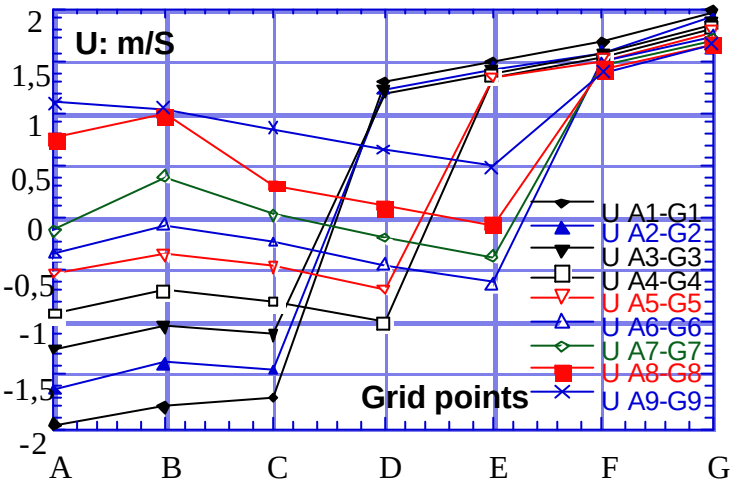

Fig. 10. U component variations along the grid columns at Y=270 deg

Concerning the U component (counted positive from the hub to the tip blade), Figure 10 presents the plot of experimental results obtained in front and behind the blade, complemented with intrapolated points around the profile. The position of the measurement volume was indeed not enough efficient (because of the beams reflexion on the blade surface) to allow a good accuracy of the U component measurement in this region. For the same reason, by use of the conservation of mass through the different surfaces of the volume V, the values of U at r+Δr have been deduced from the values at r by assuming a mean increase ΔU through the grid.

5. RESULTS AND DISCUSSION

The aerodynamic force $\vec{F} = [X, Y, Z]$ given by equation (1), has been approximated in the case of the two-bladed rotor previously defined, with :
Ψ_b =90 deg and 270 deg, $\Delta\Psi$=±5 deg;
r/R=0.7, Δ(r/R)=0.013;
μ=0.2, with V_{wt}=21.4m/s and ΩR=107.1m/s
α_s=-12 deg, and θ=10 deg.

Using the experimental results obtained on the velocity vector at each point of the grid at Ψ_b , $\Psi_b \pm \Delta\Psi$, and r/R+Δ(r/R), the integral involved in equation (1), can be calculated by help of discretized equations (2), (3) and(4).
Concerning the term $\frac{\partial(j_\infty - j_M)}{\partial t}$ its evaluation by use of equation (4) in the grid has been compared to the term $1/2(V_8^2 - V^2)$, where V is the velocity intensity in the grid plane. It can be concluded from these comparisons that :

$$4.5\%\left(\frac{1}{2}\left(V_\infty^2 - V^2\right)\right) \le \frac{\P(j_\infty - j_M)}{\P t} \le 9.3\%\left(\frac{1}{2}\left(V_\infty^2 - V^2\right)\right)$$

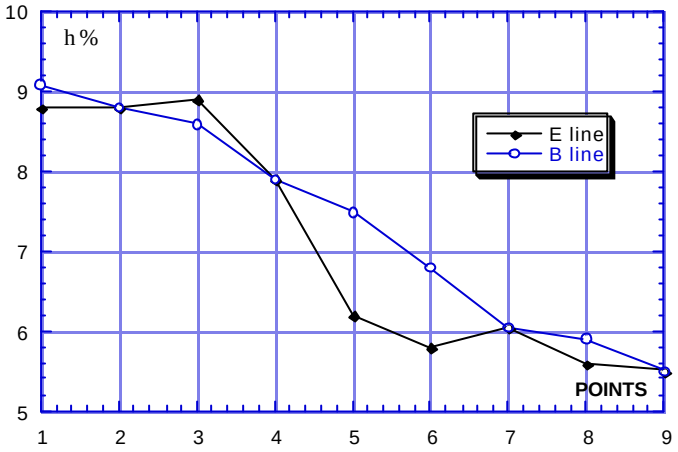

As an example, Figure 11 shows at Ψ_b = 270 deg the variation of the ratio

$$h = \left[\P(j_\infty - j_M)/\P t\right]/\left[\left(V_\infty^2 - V_M^2\right)/2\right]$$

above and below the rotating plane (lines B and E).

Fig. 11. Variations of the ratio h along the lines B and E at Y=270 deg

5.1. Evaluation of The aerodynamic forces at Y_b = 270 deg

The different values of all the terms I, II, III, and IV constituting the components of the aerodynamic force by unit span length have been summarized in the Table 1 for Ψ_b = 270 deg. The contribution ε of each term to the total component of the force is also mentionned, pointing out that the main contribution to the aerodynamic forces are generated by terms III and IV, i.e transport of momentum and pressure effects. It may also be remarked that the value of the X component is mainly due to centrifugal effects appearing in term (IV) through the variation of W between r and r+Δr.

Table 1. Components of force F at Y_b = 270 deg

$\vec{F}$ Components	X (N/m)	Y (N/m)	Z (N/m)
Term (I)	-0.121	-0.216	0.183
ε %	0.2	0.27	0.5
Term (II)	-0.39	0.005	-0.021
ε %	0;6	0.01	0.06
Term (III)	5.03	-28.81	-22.76
ε %	7;8	36.17	63.7
Term (IV)	-59.17	-50.62	12.71
ε %	91.4	63.55	35.74
FORCE $\vec{F}$=-I-II-III-IV	**54.65**	**79.45**	**9.89**

Determination of C_D and C_L coefficients.

In the plane of the grid previously defined, the coefficients C_D and C_L at r/R=0.70 can be written by help of the components Y and Z of the areodynamic force F deduced from the table 1, and the induced incidence θ_i as defined in Figure 12.

The induced incidence θ_i is given by the equation: $Arctg\theta_i = V_i/(V_{rot} - V_w)$, with : $V_w = -V_{wt}\cos\alpha_s$ where V_{wt} is the wind tunnel velocity and $V_{rot} = \Omega d\cos\beta + \Omega Ro$, β is the flapping angle, Ro the hub radius, and d the distance from the hub to the blade profile (Ro=0.11m, d=0.415m, and β=–1.29 deg at Ψ=270 deg).

V_i is the induced vertical velocity through the rotor experimentaly measured : V_i = -2,85m/s.

Lift L and drag D of the blade profile located at r/R, and the associated C_L and C_D, are given by the following equations:

$L = Y\cos\theta_i + Z\sin\theta_i$

$D = Z\cos\theta_i - L\sin\theta_i$

$$\begin{cases} C_L = \dfrac{L}{1/2\, r V_\infty^{\,2}.c} \\ C_D = \dfrac{D}{1/2\, r V_\infty^{\,2}.c} \end{cases}$$

, where V_8 is the intensity of the upstream velocity (see Figure 12).

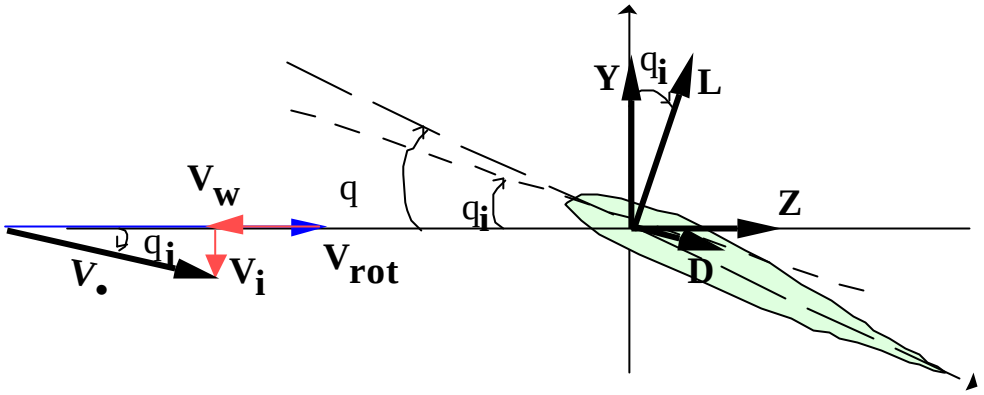

Fig. 12. Lift, drag, and induced angle of attack in the grid plane.

The first line of Table 2 shows the results obtained on lift, drag, C_L,C_D when using the 3D equation (1).

Table 2. Comparison between the different calculations of aerodynamic forces at Y_b = 270 deg.

	L(N/m)	D(N/m)	C_L	C_D	C_L/C_D
3D : Equation (1)	79.85	5.74	0.871	0.063	13.82
2D : Equation (1) limited to terms (III) and (IV) with dU/dr=0	79.96	4.67	0.873	0.051	17.12
Kutta Law $L=\rho\Gamma V_\infty$	81.1		0.884		
2D POLAR			0.757	0.049	15.45

The analysis of the different terms involved in equation (1) and presented in table 1 show that some terms can be neglected as terms (I) and (II). Moreover, if we assume that 3D effects remain light, i.e. the span variations and volume terms are neglected, the momentum equation can be applied to the contour A1A9G1G9 defined on the grid, considering a 2D flow, and involving only the velocity vector values along the contour. The so calculated quantities X and Y, give new values of L and D reported at the second line of Table 2. It can be observed that the lift is very well matched by the assumption of a 2D flow, while the drag is predicted at a value of 19% lower that the 3D case. The corresponding values of C_L and C_D are also compared in the table 2.

With the assumption of a 2D flow around the blade section, the lift can be related to the circulation by the equation of Kutta-Joukowsky: $L = \rho\Gamma V_8$, where the circulation Γ is obtained experimentally from the distribution of the velocity along the contour A1A9G1G9 by : $\Gamma = \oint_{A1A9G9G1} \vec{V}.\vec{dl}$.

The results shown at line 3 of table 2 exhibit values slightly higher than in 3D or simplified 2D configurations. However, it is worthy of note that the Kutta-Joukowski law can be applied with success to a rotor blade profile, at least in the present experimental configuration.

The last line of Table 2 gives the C_L and C_D as obtained from the 2D polar of OA209 profile, at Reynolds number $Re \approx 5.10^5$. Drag and lift coefficients are both found to be lower than in the case where the profile is in rotation.

It may be concluded from the analysis of the results in table 2 that the effects of rotation tend to increase both the lift and the drag of blade profiles resulting in a decrease of the profile aerodynamic efficiency C_D/C_L when compared to the 2D polar results, as shown at the last column of table 2.

5.2. Evaluation of the aerodynamic forces at Y_b = 90 deg

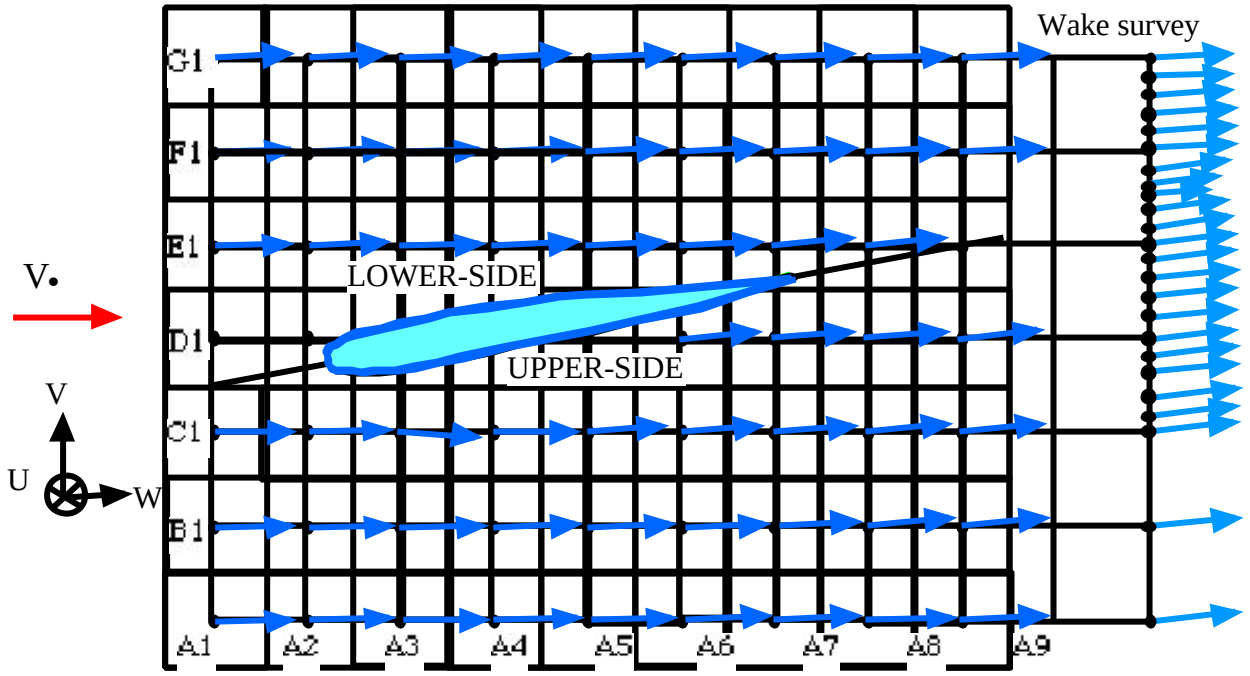

Fig. 13. Velocity results in the measurement grid at r/R = 0.7, Y = 90 deg

The evaluation of the aerodynamic forces (L, D) by unit span length at the blade azimuth Ψ_b = 90 deg is summarized in Table 3 and Figure 13 where the aerodynamic flowfield around the blade is plotted. With the assumption that the terms (I) and (II) can be neglected in equation (1), the momentum equation can be applied to the contour A1A9G1G9 defined on the grid in Figure 13. As for the Ψ_b = 270 deg case, the calculated quantities X and Y, give values of L and D reported in Table 3. The Lift coefficient obtained by means of the momentum equation is compared with the value obtained through the equation of Kutta-Joukowsky : $L = \rho\Gamma V_8$.

Table 3. Comparison between the different calculations of aerodynamic forces at Y_b = 90 deg.

	L(N/m)	D(N/m)	CL	CD
Equation (1) limited to terms III and IV.	130.7	3.71	0.462	0.014
Kutta Law : $L = \rho\Gamma V_8$	109.35		0.456	

6. CONCLUSION

The present paper has concerned a new experimental method able to measure the force components acting on the blade profile of helicopter rotors in forward flight by only use of the velocity field determined by LDV.
An effort in evaluating the relative magnitude of the different terms involved in the momentum and Bernoulli equations has been done. It has been shown that volume terms (I and II) and spanwise effects can be neglected in the momentum equation, at least in the retreating blade azimuths of the present forward flight rotor conditions. Moreover, the Kutta-Joukowsky law has been applied to the rotating profile by integrating the velocity vector along a contour surrounding the blade profile. The resulting lift is in very good agreement with the one given by the momentum equation.

The present work, involving an important experimental database, has concerned two azimuth positions of the blade (90 deg and 270 deg). Results obtained, although encouraging, have to be duplicated in the future to other phases of

rotation and other spanwise stations, in order to obtain by integration of the local forces, the resulting variation of the global forces with azimuth, particularly the drag profile acting on the blade during the rotation.

7. ACKNOWLEDGEMENT

The present results are part of a contract wich has been financially supported by "SPAE/Service des Programmes Aéronautiques", from the “Délégation Générale à l'Armement”.

8. REFERENCES

1 Landgrebe, A.J. (1986). "Overview of Helicopter Wake and Airloads Technology", Proceedings of 12th European Rotorcraft Forum, Paper n° 18, Garmish-Partenkirchen.

2 Johnson, W. (1986). "Recent Developments in Rotary Wings Aerodynamics Theory", A.I.A.A. Journal, Vol. 24, n° 8, pp. 1219-1244.

3 McCroskey, W.J. (1988). "Some Rotorcraft Applications of Computational Fluid Dynamics", Basic Rotorcraft Research, Proceedings of 2nd International Conference, pp. 1.1-1.25, Maryland.

4 Chen, C.L. and McCroskey, W.J. (1988). "Numerical Simulation of Helicopter Multibladed Rotor Flow", 18th A.I.A.A. Aerospace Sciences Meeting, A.I.A.A. Paper 88-0046, Reno.

5 Maresca, C., Favier, D. and Nsi Mba, M. (1986). "A Prescribed Radial Circulation Distribution of a Hovering Rotor Blade", Proceedings of 12th European Rotorcraft, Paper n° 23, Garmish-Partenkirchen.

6 Silva, M., Favier, D., Ramos, J., Nsi Mba, M. and Berton, E. (1993). “An Experimental Investigation of the Drag Mechanisms of a Helicopter Rotor in Hovering Flight”, Proceedings of 19th European Rotorcraft, Paper n°18, Cernobbio.

7 Ramos, J., Nsi Mba, M., Berton, E., Favier, D. and Silva, M. (1994). “A Laser Velocimetric Investigation of the Airloads and Performance of a Model Helicopter Rotor in Hover”, American Helicopter Society Aeromechanics Specialists Conference, Paper n° 8.1, San Francisco.

8 Berton, E., Favier, D., Maresca, C. and Nsi Mba, M. (1994). “A New Method of Laser Velocimetry for Airloads Determination on Hovering Rotor Blades” ICAS-AIAA, Proceedings of 19th Congress of Aeronautical Sciences, ICAS Paper n °94-353, pp. 1610-1619, Anaheim.

9 Berton, E., Favier, D., Maresca, C. and Nsi Mba, M. (1994). “Airloads Determination on the Hovering Rotor Using a Laser Velocimetry Technique”, AGARD, 75th Fluid Dynamics Panel Meeting and Symposium on Aerodynamics and Aeroacoustics of rotorcraft, AGARD CP N°. 552, Berlin.

10 McAlister,K.W., Schuler, C.A., Branum, L., and WU, J.C. (1995). “3-D Wake Measurement Near a Hovering Rotor for Determining Profile and induced Drag“, NASA Technical Paper 357.